

Original papers

Assessing the impact of soil and field conditions on cotton crop emergence using UAV-based imagery

Fengkai Tian^a, Curtis J. Ransom^b, Jianfeng Zhou^{c,*}, Bradley Wilson^d, Kenneth A. Sudduth^b^a Department of Chemical and Biomedical Engineering, University of Missouri, Columbia, MO 65211, USA^b Cropping Systems & Water Quality Research Unit, USDA-ARS, Columbia, MO 65211, USA^c Division of Plant Science and Technology, University of Missouri, Columbia, MO 65211, USA^d Fisher Delta Research, Extension, and Education Center, University of Missouri, Portageville, MO 63873, USA

ARTICLE INFO

ABSTRACT

Keywords:

Cotton
Stand count
Emergency uniformity
Remote sensing
Precision agriculture

Crop seeding rate is one of the crucial factors that affect crop production. However, acquiring adequate crop data in multiple growing environments is time-consuming and challenging in large fields. This study aimed to develop and evaluate an efficient method using an unmanned aerial vehicle (UAV) imaging system and deep learning to assess cotton emergence spacing uniformity at different seeding rates. The study was conducted on a 3.27-hectare research field planted with two cotton cultivars at five seeding rates (56 k, 74 k, 91 k, 108 k, and 123 k seeds ha^{-1}), with each treatment containing four rows with three replicates in a random block design. A UAV imaging system collected RGB images at 10 m and 15 m flight height above the ground level at two and six weeks after planting. Orthomosaic images from the two days were segmented into small blocks that were processed using the object detection algorithm YOLOv7 to identify cotton plants. Hough transform and polynomial regression were used to identify each cotton row and remove weeds. The number of plants in each 5-m row segment (i.e., stand count) was calculated to correlate with soil electrical conductivity (EC_a) and field elevation. Results show that the research could detect cotton plants with the mean average precision of 96.9 % at the 50 % intersection over the union threshold (mAP@50) for the two-week dataset and 92.7 % mAP@50 for the six-week dataset. The results also show that plant uniformity was closely correlated with field elevation and EC_a , with an average R^2 of 0.62 using the Random Forest model. The coefficient of variation was used to evaluate the spacing uniformity of each seeding rate and demonstrated that the seed rates of 108 k and 123 k seeds ha^{-1} tended to exhibit better spacing uniformity than others under various environmental conditions. This study provides valuable insights by developing a pipeline for early-stage cotton stand count using high-resolution remote sensing techniques to evaluate the uniformity of different seeding rates for cotton, ultimately improving the efficiency of crop management.

1. Introduction

Cotton (*Gossypium hirsutum* L.) is one of the most widely planted cash crops worldwide, with an anticipated production of 25 million tons in 2023 (Walker, 2023). Cotton production is vulnerable to climate changes (e.g., changing temperatures and inconsistent water supply) and soil constraints (e.g., soil salinity and poor drainage) (Kholliyev et al., 2020; Sankaranarayanan et al., 2010). Soil condition is one of the important environmental factors that may substantially affect crop productivity (Liliane & Charles, 2020). Soil with poor structural properties can negatively affect seed vigor, affecting plant spacing uniformity (Sonon et al., 2015). Field topographic features affect soil physical,

chemical, and hydrological features that also affect crop seed germination (Harper et al., 1965). Therefore, field topography and soil information need to be considered when making planting decisions to improve crop emergence and optimize seeding rates.

Precision crop management strategies can reduce the limiting effects of soil and field topography on crop production. For example, research has shown that optimizing the seeding rate of cotton to match the growing constraints could improve lint yield and economic returns (Adams et al., 2019). However, the quantitative correlation between cotton yield, soil conditions, and field topography was not clear. One of the challenges to determining the quantitative effects of environmental factors on crop yield is the lack of efficient tools for assessing crop

* Corresponding author.

E-mail address: zhoujianf@missouri.edu (J. Zhou).

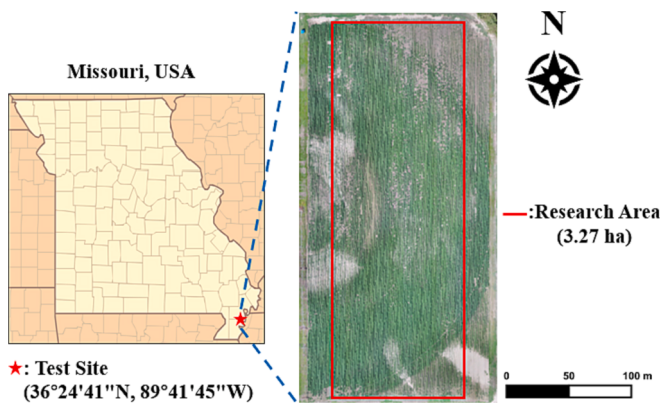


Fig. 1. Study site and research area.

emergence and stand count. The conventional approach to evaluating cotton stands requires farmers to manually count cotton plants within small defined areas replicated a few times within a field (Butler, 2019). However, manual stand count is time-consuming and labor-intensive, which results in low spatial sampling resolution and human errors. Recent work monitored crop stand count and spacing heterogeneity by employing a ground-based mobile platform to collect the image data, especially for early emerged plants (Liu et al., 2017; Wang et al., 2021). However, ground-based mobile systems may be challenging to operate in large fields due to uneven terrain and travel speed.

Remote sensing technology can efficiently collect high-resolution temporal, spatial, and spectral data of crops in a large area (Maes & Steppe, 2019). In recent years, unmanned aerial vehicle (UAV)-based remote sensing systems have been widely used in agricultural research and applications as a high-throughput data collection tool (Tsouros et al., 2019). Compared to satellite-based remote sensing, UAV systems have the advantages of compact size, flexible data acquisition time, and easy access to high-resolution imagery data with customized imagers (Bouguettaya et al., 2022). Recent studies have demonstrated the potential of utilizing red, green, and blue (RGB) cameras mounted on UAVs for various digital agriculture applications across different crops. Some related applications of RGB images include assessing stand count (Liu et al., 2022; Vong et al., 2021), identifying weeds (Khan et al., 2021; Lottes et al., 2017), estimating yield (Feng et al., 2023; Zhang et al., 2020b), detecting crop pests (Kaivosoja et al., 2021; Tetila et al., 2020), and evaluating plant traits (Tian et al., 2023; Zhang et al., 2019).

The advancement of computer vision and high-performance computing has substantially enhanced the application of UAV imagery in agriculture. Emerging data analysis methods, such as machine learning and deep learning algorithms, have been applied in agriculture-related tasks. Pre-trained deep learning models have been applied to analyze complex agricultural data, resulting in more efficient and cost-effective crop management practices (Sharma et al., 2020). YOLO and the R-CNN family represent one-stage and two-stage object detection algorithms (Diwan et al., 2023). Both types of algorithms can be developed with different levels of model complexity for various applications, depending on the computational speed and desired accuracy level. These two types of algorithms have been applied to field UAV imagery for crop stand count analysis in sunflower (Fuentes-Penailillo et al., 2019), corn (Vong et al., 2021), potato (Li et al., 2019), and rapeseed (Zhang et al., 2020a). In addition, similar studies estimated crop density (Jin et al., 2017), plant germination (Li et al., 2019), and canopy cover (Feng et al., 2020). Nevertheless, many of these studies only observed crops on a certain day and did not integrate the result from the UAV with ground environmental factors.

This study aimed to investigate the potential of using a UAV imaging system for estimating cotton spacing uniformity at different seeding rates and field conditions. The three primary objectives included: (1) to

Table 1
Flight information and temperature for the two dates of data acquisition.

Information	June 01, 2022 (17 days after planting)	June 20, 2022 (37 days after planting)
Flight Height	10 m	15 m
Flying Speed	1.2 m s ⁻¹	1.8 m s ⁻¹
Snapshot frequency	2 s	2 s
Forward Overlap	75 %	75 %
Sideward Overlap	70 %	75 %
GSD*	2.2 mm pixel ⁻¹	3.5 mm pixel ⁻¹
Temperature	≈ 25°C	≈ 34°C

GSD*: Ground Sampling Distance (mm pixel⁻¹) generated by image stitching software: Agisoft Metashape®.

develop a deep learning model for assessing cotton stand count at two growth stages, (2) to examine the effect of soil conditions and field elevation on cotton emergence uniformity at five seeding rates, and (3) to identify the optimal cotton seeding rate in field areas with different field conditions to achieve uniform crop emergence.

2. Materials and methods

2.1. Field experiment

This study was conducted in a cotton field at the Fisher Delta Research, Extension, and Education Center of the University of Missouri, located in the upper Mississippi River delta near Portageville, MO, USA (Fig. 1, 36°25'47"N, 89°42'4"W). The dimensions of the research field were approximately 295 m (N-S) by 111 m (E-W) with an area of 3.3 ha. Due to the combined influences of alluvial deposits and tectonic stresses, the field exhibits considerable spatial variability in soil texture. Therefore, apparent soil electrical conductivity (EC_a) was collected using a Veris 3100 instrument (Veris Technologies Inc., KS, USA) throughout the entire field, resulting in a total of 2,757 EC_a data points. The EC_a measurements were used as an indirect indicator of soil texture and quality (Sudduth et al., 2003). In addition, the field elevation was measured using a mobile Global Navigation Satellite System (GNSS) receiver (Geo 7X, Trimble Navigation Ltd., CO, USA) mounted on a UTV while collecting EC_a data. There were 7,565 GNSS readings acquired in the research field that were used to map the field's topography. Two cotton cultivars, ST 4990B3XF and ST 5091B3XF (BASF SE, Mannheim, Germany), were planted at a row spacing of 0.93 m on bedded soil using a commercial planter (John Deere 1700, Moline, IL USA) at five different seeding rates (i.e., 56,834, 74,131, 91,429, 108,726, and 123,552 seeds ha⁻¹), labeled as 56 k, 74 k, 91 k, 108 k, and 123 k, on May 16, 2022. Each treatment (cultivar by seeding rate) was planted as a four-row field-length pass with three replicates based on a random block design, resulting in a total of 30 passes or 120 cotton rows in the N-S.

2.2. Imagery data collection

Imagery data was acquired using a UAV platform (Phantom 4 Advanced +, DJI Technology Co Ltd., Guangdong, China) equipped with an RGB camera having a resolution of 5472 × 3648 pixels. Each image frame was geo-referenced by the UAV's onboard GPS. A flight planning application Litchi (VC Technology Ltd., London, UK) installed on an iPad Mini 4 (Apple Inc., CA, USA) was used to configure flight parameters (i.e., height, speed, frame rate). The app was also used to design flight paths for the UAV to ensure sufficient image overlap (>70 %) and complete field coverage. Table 1 provides the details of the flight configurations and the ambient air temperature during the two data collections. All the data was collected at around noon with a clear sky.

Twenty-one Ground Control Points (GCPs) were deployed randomly throughout the study area. The GCPs were made of 1.0-m fence posts with a white and black-colored square board of 32 cm × 32 cm fastened on top (Fig. 2a). Ten quadrats were deployed randomly in the field as

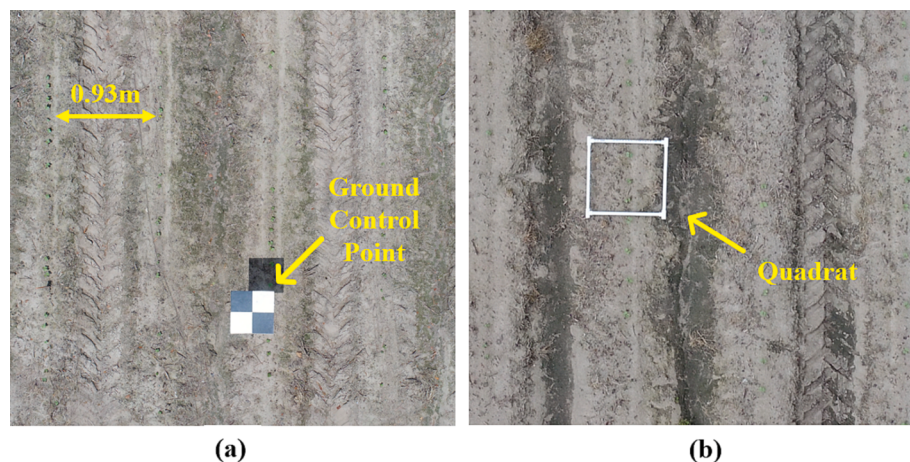


Fig. 2. An example of a ground control point (GCP) and a quadrat used in the UAV imagery data collection. (a) A GCP made of a fence post and cross-color pattern top was used to increase the positioning accuracy. (b) A quadrat made of a PVC pipe was used to calibrate the ground sampling distance.

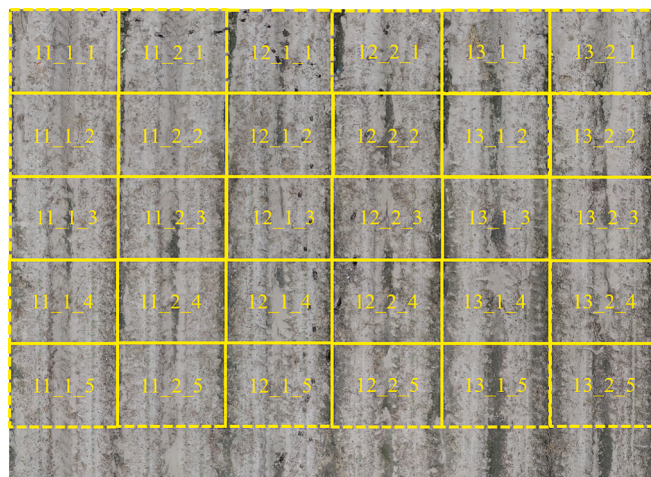


Fig. 3. Illustration of the sub-plots cropped from each segmented image. The numbers in the sub-plots follow the naming convention used for object detection in the deep learning method.

references for the Ground Sampling Distance (GSD). The quadrats were constructed using polyvinyl chloride (PVC) pipes with an inner dimension of $0.5\text{ m} \times 0.5\text{ m}$ (Fig. 2b). A real-time kinematic (RTK) GNSS system Reach RS+ (EMLID Ltd., Budapest, Hungary) was used to obtain the coordinates of both GCPs and GSD quadrats at a position error of less than 0.02 m.

2.3. Data pre-processing

The digital aerial image processing software Agisoft Metashape (Agisoft LLC, St. Petersburg, Russia) was used to stitch UAV images to generate orthomosaic images using the software's recommended protocol (Agisoft, 2014). All GCPs were utilized to correct or adjust the geolocation of images. The orthomosaic images were exported as a 'tiff' (Tag Image File Format) file and processed using the Image Processing Toolbox and the Computer Vision System Toolbox of MATLAB (ver. 2022a, MathWorks, MA, USA) to segment each pass (four crop rows) from the orthomosaic image based on the cotton row number. The 30 segmented images were labeled from 1 to 30, corresponding to the ten treatments of two cultivars by five seeding rates with three replicates.

Each pass consisted of four rows of cotton and was divided into subplots of identical dimensions within each day, i.e., dataset 1: 640×800 pixels and day 2: 640×540 pixels. The sub-plots, each comprising a portion of two rows of cotton, were then resized to a dimension of 640×640 pixels according to the requirement of the deep learning model. The resizing was performed using the Python function "cv2.resize" with the interpolation method of "INTER_NEAREST", which provides fast results with fewer computing resources by rounding the pixel values of the resized image to the nearest integer. This interpolation method provided good results in this study because the variation among neighboring pixels was relatively small due to the high spatial resolution. Therefore, it was expected that results with the simple method would only be slightly different than with other, more complex methods (e.g., INTER_CUBIC). As shown in Fig. 3, each segmented sub-image was stored and labeled based on its position, i.e., the sequence number of passes from west to east (No.pass), sub-plot in the pass (No.column), and sequence number of sub-plots from north to south (No.row).

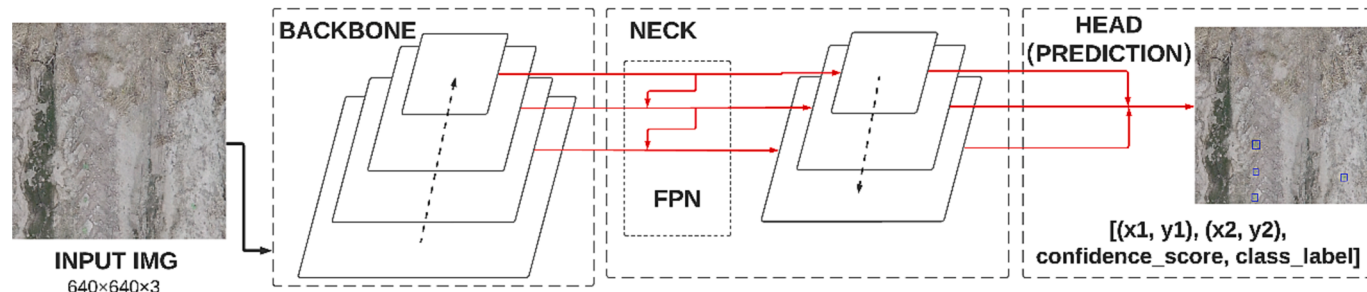


Fig. 4. An overview of the YOLOv7 prediction pipeline. The architecture consisted of three components: the backbone extracts features from an input image, the neck creates feature pyramids for different scales, and the head outputs the detected object information.

Table 2

Hyperparameters used for YOLOv7 model training in this study.

Training hyperparameter	Value
Max epochs	200
Batch size	6
Initial learning rate	0.01
Weight decay	0.0005

2.4. Framework of cotton stand count and uniformity evaluation

The deep learning model YOLOv7 (Wang et al., 2022) was used to detect cotton plants from images of sub-plots. This recently released model within the YOLO series was designed for object detection. YOLOv7 requires significantly less computing power than other deep learning models and outperformed existing one-stage and two-stage object detection models for detecting weeds in UAV images (Gallo et al., 2023). Additionally, this model provides a more efficient, robust, and faster network architecture, which facilitates rapid inferences and enhanced detection accuracy by introducing several architectural reforms, such as E-ELAN (Extended Efficient Layer Aggregation Network) and model scaling techniques (Panigrahy & Karmakar, 2022). The architecture of YOLOv7 is primarily composed of three parts, i.e., the backbone, neck, and head (prediction) networks (Fig. 4). The backbone network extracts the most important image features, while the neck network fuses this information to produce a set of feature maps, constructing the feature pyramids network (FPN). Lastly, the head network consists of output layers for predicting the pixel position of bounding boxes for each object class, along with a confidence score that represents the probability of the predicted bounding box containing the cotton. Fig. 4 visualizes the YOLOv7 model architecture. The training hyperparameters summarized in Table 2 were selected based on a preliminary trial.

Cotton plants were manually labeled using an online tool, Roboflow (Dwyer & Nelson, 2022). The dataset for the first flight (June 1) included 2,492 labeled cotton plants from 275 images that were randomly selected from 12,243 images (sub-plots). The dataset for the second flight (June 20) consisted of 3,791 labeled cotton plants from 226 images randomly selected from 7,911 sub-plots. Both training and testing datasets contained images of all cotton seeding rates that were randomly selected from across the field to reduce the effect of soil conditions. Both datasets (June 1 and 20, hereafter referred to as Dataset 1 and 2) were partitioned into separate training (80 %) and testing (20 %) datasets. To reduce the potential bias in model performance, the training dataset included images that were manually selected to ensure sample representation from all areas of the field. This approach ensured that the

datasets were balanced in terms of various environmental factors. Models were trained and tested separately for the two image datasets.

A text file was established for each labeled image to record the class id and the location (coordinates) of each bounding box for the detected cotton plants. The content was encoded in the following order: “id”, “x_min”, “y_min”, “x_max”, and “y_max”, indicated by the image filename and four values in pixels. The rest of the unannotated images were processed using the trained YOLOv7 model. A comma-separated value (.csv) file of each image containing the bounding boxes’ position information was recorded as the coordinates [x_{min}, y_{min}, x_{max}, y_{max}, confidence score] of each bounding box. The confidence score was calculated using a sigmoid function which generates a score that represents the probability that the bounding box contains an object. To reduce the occurrence of false positives (FP), bounding boxes with confidence scores lower than 0.3 were excluded. The pixel positions of the rest of the bounding boxes were then calculated and updated according to their file names with Eqs. (1) and (2).

$$x_k = x_i + \sum_{nc=1}^i [640(nc - 1)] \quad (1)$$

$$y_k = y_j + \sum_{nr=1}^j [640(nr - 1)] \quad (2)$$

where $x_i \in \{x_{min}, x_{max}\}$, $y_i \in \{y_{min}, y_{max}\}$, nc = No.column (the sub-plot number in each pass), nr = No.row (sequence number of the sub-plots from north to south), $i = 1, 2$, sub-plot in each pass, j = Max value of nr . Updated coordinates of a position were saved as $[x_k, y_k]$.

The above steps updated and recorded the coordinates for each identified cotton plant. The center of each bounding box $[x_3, y_3]$ was calculated by adding half of the box’s width to the x-coordinate, and half of the height to the y-coordinate of the top-left corner pixel position. A k-means clustering algorithm from the *scikit-learn* package (version 1.2.2) (Pedregosa et al., 2011) was used to classify the detected plants from rows 1 to 4 of each pass based on the pixel position $[x_3, y_3]$ of each object.

Among the plants detected were cotton and weeds, the latter of which needed to be removed. In this study, most of the weeds were between the cotton rows. Therefore, the Standard Hough Transform (SHT) (Duda & Hart, 1972) was used to detect plant rows and plants that were not in the row were considered weeds. The function “*HoughLinesP*” from the OpenCV package in Python (version 3.9.16) was used to detect cotton rows in binary images, where “1” denotes the pixels within bounding boxes, and “0” was used to indicate the result of the pixels. Bounding boxes that were not intersected by lines detected using the SHT were assumed to be weeds and deleted as shown in Fig. 5a. Since the cotton rows were not completely straight, some weeds might not be removed if a straight line was used to represent the cotton row. To

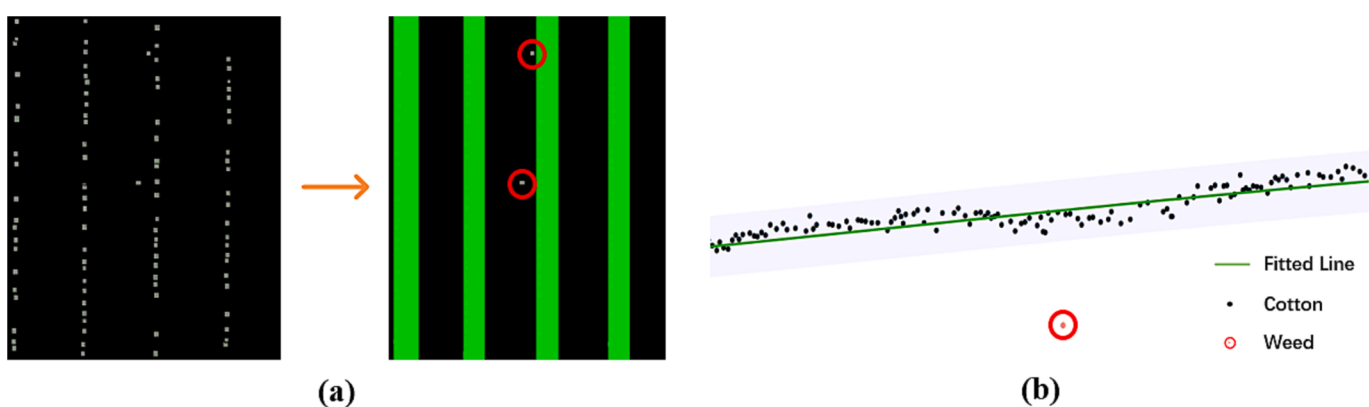


Fig. 5. Demonstration of weed removal using a line-detection technique. (a) An RGB image of a portion of four cotton rows (one pass). After applying the SHT, two objects (highlighted by red circles) not aligned with the row have been detected. (b) A scatter plot of a segment of a single cotton row. Following the polynomial regression (degree = 4), one object (indicated by a red circle) outside the 95 % correlation prediction interval was identified.

address this issue, a fourth-degree polynomial regression was used to fit each cotton row into three parts (0 ~ 100 m, 100 ~ 200 m, and 200 ~ 295 m). The 95 % prediction interval was calculated using the function “predict.lm” from the base package “stats” in R (version 4.2.2). Points outside the upper and lower bounds of the interval were considered weeds and removed, as shown in Fig. 5b. Combining both the SHT and the polynomial regression was expected to improve the performance of weed extraction.

This study aimed to evaluate the spacing uniformity rather than the spatial distribution of cotton plants, therefore, it is important to measure the distance between two adjacent cotton plants along a row (i.e., the y-axis). The plant spacing in pixel number was calculated using the distance between pixel positions $[x_3, y_3]$ of two plants, which was converted to millimeters using the GSD.

The performance of YOLOv7 in cotton plant detection was evaluated using the mean average precision (mAP@50), with an intersection over union (IoU) threshold of 0.50 (PASCAL VOC metric (Rezatofighi et al., 2019)). The calculation of mAP@50 provided by (Padilla et al., 2021) involves the performance metrics of Precision, Recall, and Average Precision (AP), as defined in Eqs. 3—5. In addition, the coefficient of determination (R^2) was used to measure the strength of the linear relationship between true and predicted values, providing another assessment method for the predictive model on testing datasets.

$$\text{Precision} = \frac{TP}{TP + FP} \times 100\% \quad (3)$$

$$\text{Recall} = \frac{TP}{TP + FN} \times 100\% \quad (4)$$

$$AP = \int_0^1 \text{Precision}(Recall) \quad (5)$$

$$R^2 = 1 - \frac{\sum_i (y_i - \hat{y}_i)^2}{\sum_i (y_i - \bar{y})^2} \quad (6)$$

where, TP = True Positive, indicates the number of correctly detected cotton plants with an IoU of 0.5 or higher. FP = False Positive, indicates the number of non-cotton objects that were detected as cotton plants (IoU lower than 0.5), where the predicted bounding box is a duplicate detection for the same ground truth. FN = False Negative, is the number of cotton plants that were undetected by the algorithm, meaning there is no predicted bounding box with an IoU of 0.5 or higher. The \hat{y} represents the number of detected cotton plants in each image, y indicates the number of manually counted objects on each image, and \bar{y} is the sample mean. Imagery data processing and model implementation were conducted on Google Collaboratory (Google LLC, CA, USA) and a desktop PC configured with an Intel (R) Core i7-12700 CPU, 32 GB RAM, with a 256 GB solid-state drive.

The spacing uniformity of cotton in 5-m row segments at five different seeding rates was evaluated using the coefficient of variation (CV) as defined in Eq. (7). The CV compares sets of continuous values at various scales and magnitudes (Brown, 1998). A lower CV value indicates higher uniformity.

Table 3

Performance of YOLOv7 model in cotton detection using images collected in two days.

Metric	Dataset 1 (June 01, 2022)	Dataset 2 (June 20, 2022)
Training dataset	220 images ($n^2 = 1920$)	181 images ($n = 2889$)
Testing dataset	55 images ($n = 572$)	45 images ($n = 902$)
mAP@50 ¹	96.8 %	91.7 %
mAP@50 after weeds deleted	96.9 %	92.7 %
R^2	0.93	0.93

¹ Based on the testing dataset. ² Total number of labeled cotton plants.

$$CV = \frac{\sigma}{\mu} \times 100 \quad (7)$$

where, σ and μ represent the standard deviation and the mean of the number of cotton plants in each 5-m segment, respectively.

2.5. Data georeferencing

In section 2.4, the segmented images were resized to be used as inputs for the YOLOv7 model. However, the resized images changed the associated geospatial information of the detected cotton plants. An image processing approach was developed to recover the geospatial information using the following procedures. Firstly, the bounding boxes were rescaled to match the original image size using “resize_image-with_bbox” from the Chitra package (version 0.2.0) in Python. Then, a function “GetGeoTransform” from the Python package rasterio (version 1.3.6) was used to convert the $[x_3, y_3]$ of each bounding box to the GNNS coordinate reference system (CRS) (i.e., latitude, longitude). This step ensured each plant was geo-referenced to align with the orthomosaic image.

The cotton plants detected from aerial imagery were geo-referenced and analyzed using QGIS (version 3.28.2 - Firenze). The cotton was then aligned with ground data to conduct a quantitative analysis of spacing uniformity at different seeding rates and ground environment factors. We used the inverse distance weighting (IDW) interpolation method instead of ordinary kriging (OK), because OK has a smoothing effect, which may result in a negative impact on a dataset with high spatial variability, and the semivariogram construction is more subjective (Qiao et al., 2018). A polygon layer covering the entire research area was first created, and then ground environment data were interpolated using the built-in function “IDW interpolation” from QGIS. The IDW assigned estimated EC_a and elevation data to each detected cotton plant using Eq. (8).

$$W_{(x)} = \frac{\sum_i^N W_i}{\sum_i^N d_i^{-\alpha}} \quad (8)$$

where, the $W_{(x)}$ is predicted value; N represents the total number of data points; W_i is i^{th} data value; d_i is the Euclidean distance between point i and x ; The distance coefficient, α , was set to the value of 2 (default).

2.6. Statistical analysis

After calculating the distance between each cotton plant and its neighbors within each cotton row, each cotton row was divided into 59 5-m segments to count the number of cotton plants within each segment. The data was then organized into a matrix with 59 rows and 120 columns. The analysis of variance (ANOVA) test was employed to determine the statistical significance of the difference in the number of cotton plants in a 5-m row segment between the top 10 % of soil EC_a values and the bottom 10 % of soil EC_a values across each of the five seeding rates. The function “aov” in R was used for statistical analysis. A “p-value” ≤ 0.05 was used to indicate a significant difference.

Mean values of soil EC_a and field elevation were calculated for each 5-m segment to analyze their statistical relationship with the number of cotton plants (No. cotton) under different seeding rates. A higher No. cotton indicates a greater density and vice versa. The ordinary least squares (OLS) and random forest (RF) statistical models were applied as linear and non-linear statistical models with default parameters. The dependent variable was the stand count within each 5-m segment for each seeding rate, while the associated elevation and EC_a were the independent variables. The coefficient of determination (R^2) was used to assess the effectiveness of the model in capturing and explaining the underlying patterns in the data.

The spacing uniformity of each seeding rate in the presence of similar ground environmental factors was also worth investigating. First, we

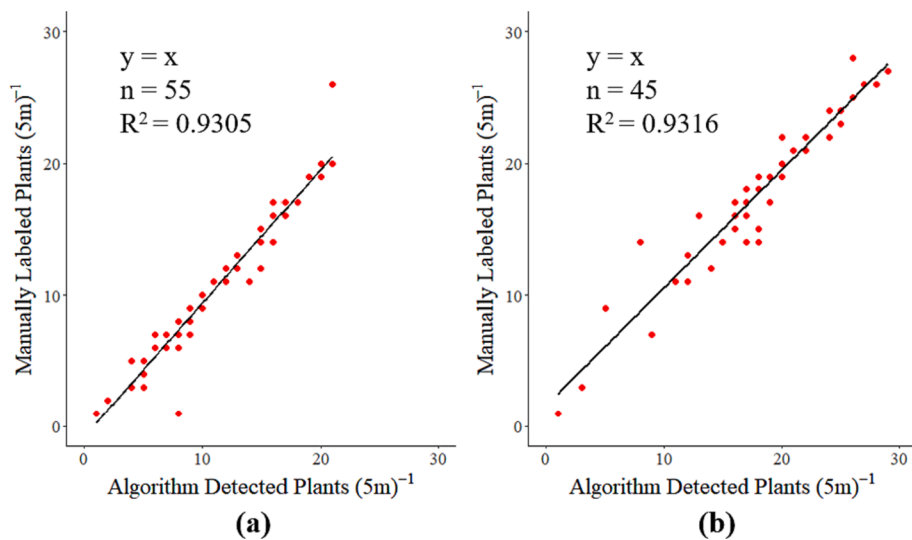


Fig. 6. Comparison between manual and image-based stand count for (a) Dataset 1 and (b) Dataset 2.

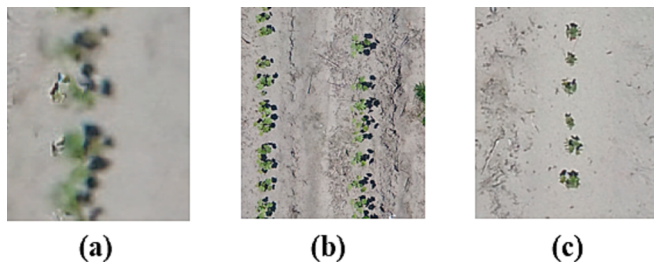


Fig. 7. Illustration of potential data collection issues (image from Day 2). (a) A blurred image was potentially caused by wind or limitations of the image stitching software. (b) Shadows in aerial photos were caused by the position of the sun. (c) Late emergence or slower growth caused cotton canopy size variations.

divided the elevation and soil EC_a data into quintiles, with each part representing 20 % of the numerical value range. Next, we calculated the distance between each cotton plant and its neighbors for all five seeding rates and then computed the coefficient of variation based on the quintiles of ground environmental factors.

3. Results and discussion

3.1. Cotton plant detection

The performance of the YOLOv7 model in detecting cotton plants using the imagery datasets of both days is shown in Table 3. The mAP@50 for both days was greater than > 91 %. The table also shows that the mAP@50 for both days would increase by 0.1 % and 1.0 % for dataset 1 and 2 if weeds were removed using the technique described in section 2.4.

Fig. 6 illustrates the agreement between the stand count of each 5-m row segment as detected by the model and the manually labeled data. The R² was calculated using the dataset after removing weeds. Although dataset 1 demonstrates a higher mAP@50 than dataset 2, there is no obvious difference across both image datasets when we use R² as an evaluation metric.

Throughout the field, several factors could influence the training of the model. Fig. 7a shows that a part of the image (cotton leaves) is slightly blurred, which could be due to wind moving cotton leaves or affecting the UAV or limitations of the image stitching software. Fig. 7b displays that as the cotton plants grow taller, shadows became more noticeable in images compared to earlier images. Fig. 7c illustrates that some cotton plants either emerged later or grew more slowly than others since there is an obvious difference in canopy size between plants at the

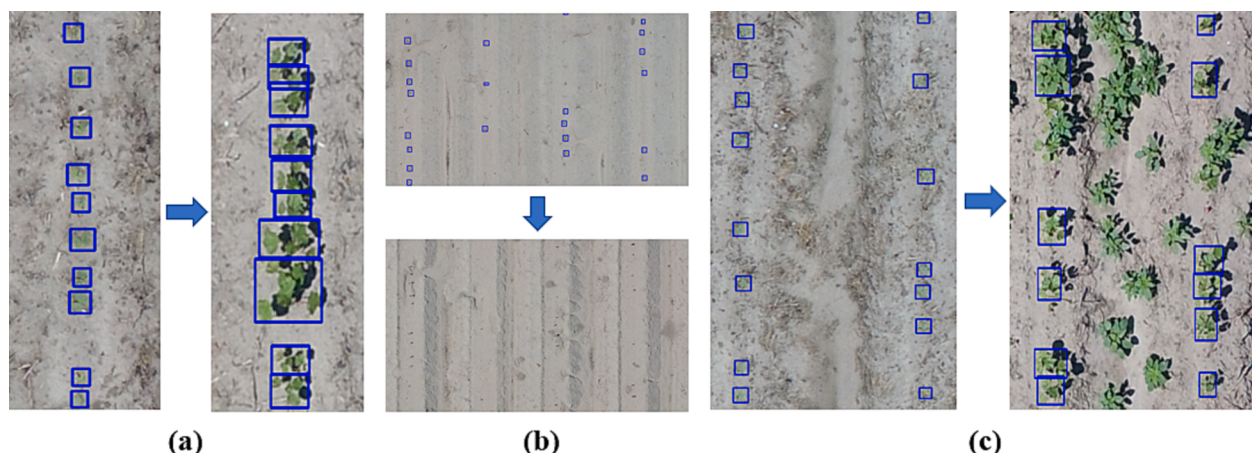


Fig. 8. Comparison of emerged plants at the same locations in two days (Day 1 and Day 2). (a) Variation of canopy size at two days caused challenges in labeling and detecting individual plants. (b) Emerged plants were detected on Day 1, but some died on Day 2. (c) Weeds may increase both false negative and positive errors.

Table 4

Means and standard deviation (mean \pm std) of cotton stand count of the test cultivars in one pass (four rows) quantified by images collected in two days.

Seeding Rate	Stand count of each pass				Difference between two days (Day 1 - Day 2)	
	Day 1 (June 01, 2022)		Day 2 (June 20, 2022)		ST 4990	ST 5091
	ST 4990 ¹	ST 5091 ²	ST 4990	ST 5091		
56 k	3,451 \pm 180	3,913 \pm 351	3,635 \pm 230	4,125 \pm 379	-185 \pm 61	-212 \pm 85
74 k	4,228 \pm 162	4,867 \pm 607	4,186 \pm 115	4,981 \pm 614	41 \pm 226	-115 \pm 99
91 k	4,933 \pm 640	6,490 \pm 241	5,030 \pm 516	6,090 \pm 496	-98 \pm 686	400 \pm 281
108 k	6,983 \pm 1,158	7,632 \pm 1,413	8,173 \pm 0*	6,794 \pm 1,516	447 \pm 0*	837 \pm 217
123 k	7,471 \pm 1,617	9,439 \pm 405	6,981 \pm 1,416*	7,996 \pm 599*	261 \pm 46*	1,545 \pm 135

* Data was not collected for four passes on day 2 due to a technical issue. ¹ST 4990B3XF. ²ST 5091B3XF.

second data collection date. Although the variations in image quality, plant size, and shadow had the potential to introduce bias into the model's performance, the training dataset was manually selected across the whole field. This approach ensures that the dataset is balanced in terms of different types of soil and field elevations.

3.2. Stand count of different treatments

Cotton plants exhibit different characteristics at different growth stages, such as germination, leaf and canopy development, and boll development (Oosterhuis, 1990). The cotyledons of cotton plants were visible in the images at the first data collection event. In some rare cases, groups of cotton plants were clustered together, possibly due to the performance of the planter (e.g., doubles). However, in most areas,

individual cotton plants could be clearly and easily identified visually in aerial images on the first data collection. The growth stages of the plants at locations varied, which might be due to the variation in soil conditions.

As shown in Fig. 8a, even within the same area, some cotton plants had a larger canopy size and more leaves than others. In contrast to the first dataset, we found that some cotton plants with large canopy sizes can obscure or block the view of the smaller ones by the time of the second data collection. The overlap of cotton plant canopies increased the likelihood of mislabeling cotton plants, which further decreased the model's performance on the second dataset. Fig. 8b also shows the same location on different dates. We noticed that there were some areas where many cotton plants successfully emerged from the soil as seen in the first data collection event but did not survive. This could potentially lead to a reduction in the number of detected cotton plants on the second day. On the other hand, Fig. 8c shows that weeds developed in some areas during the second data collection, contributing to a lower accuracy of plant detection. Although we could remove weeds based on the line detection techniques, weeds in cotton rows were mistakenly identified as cotton by the algorithm. Moreover, as plants grow larger leaves and canopies, especially in dense areas, both the detection algorithm and human observers may mistakenly identify two adjacent plants as one.

Higher seeding rates (108 k and 123 k seeds ha^{-1}) resulted in higher stand counts and standard deviations than lower seeding rates (56 k and 74 k seeds ha^{-1}) on both data collection dates (Table 4). There was a notable difference between the stand counts observed on both sampling days with more cotton plants observed at the lower seeding rates on the second day (as observed by negative values in Table 4). However, at higher seeding rates, the opposite was true. The variables in stand count between dataset 1 and dataset 2 across different seeding rates and cultivars reveal the potential effect of environmental factors on cotton stand count and spacing uniformity in this study.

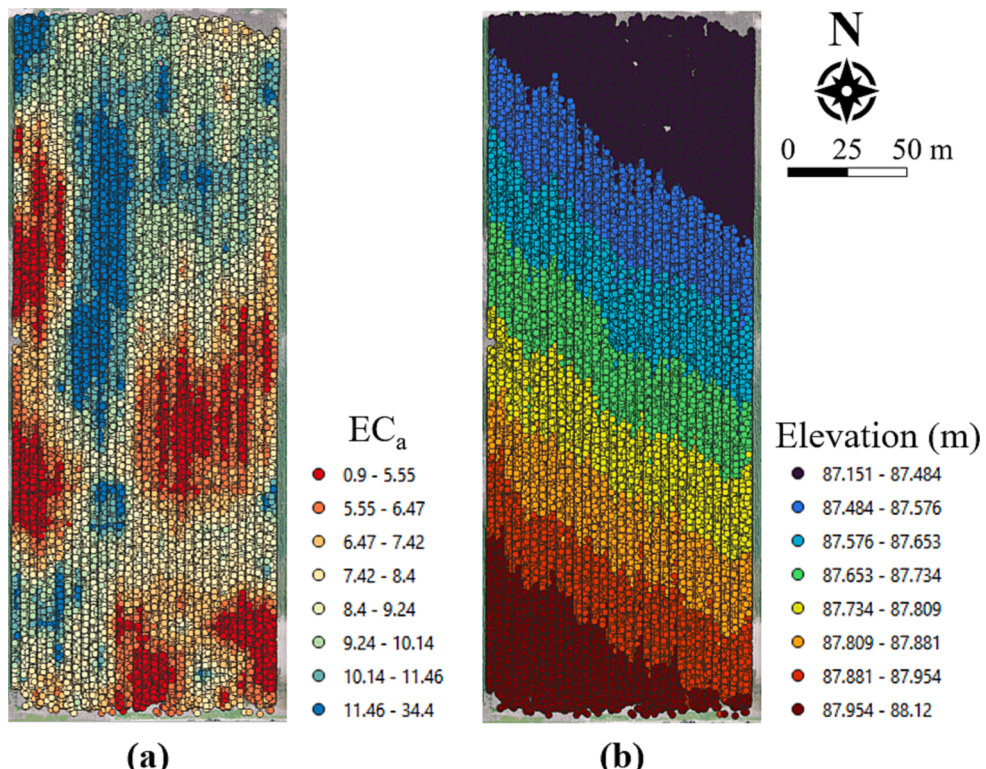


Fig. 9. Maps of (a) shallow EC_a (0—30 cm) at the location of each cotton plant with low and high EC_a values associated with sandy and clay textures and (b) field elevation.

Table 5

The strength (R^2) of the statistical relationships between independent variables (soil EC_a and field elevation) and cotton stand count.

Statistical Model	Seeding Rate				
	56 k	74 k	91 k	108 k	123 k
Ordinary Least Squares	0.242	0.202	0.197	0.375	0.174
Random Forest	0.597	0.573	0.642	0.685	0.589

Table 6

Comparison of target seeding rates and actual stand count per row.

Parameters	Seeding Rate				
	56 k	74 k	91 k	108 k	123 k
Target number of seeds per row	1642	2142	2642	3142	3571
Average stand count per row	918	1131	1459	1824	2110
Overall plant establishment rate (%)	55.9	52.8	55.2	58.1	59.1
ST 4990B3XF Plant establishment rate (%)	59.4	56.5	61.1	60.1	66.0
ST 5091B3XF Plant establishment rate (%)	52.3	49.2	49.4	55.6	52.2

3.3. Impact of soil type and field elevation on plant spacing uniformity

The impact of field elevation and soil EC_a on cotton stand count and spacing uniformity was evaluated using dataset 1 due to the higher mAP@50. A total of 178,677 cotton plants were detected in the research area. The shallow EC_a (0 to 30 cm) data ranged from 0.91 to 34.39, with a median value of 8.00 and a sample standard deviation of 4.38. Fig. 9a visualizes the EC_a assigned to each cotton plant using IDW interpolation. Lower EC_a values are usually related to soils with high sand content and low organic matter, while higher EC_a values are commonly related to soil with high clay content (Friedman, 2005). The elevation data ranged from 87.06 m to 88.29 m with a median value of 87.66 m and a standard deviation of 0.29 m. Fig. 9b visualizes the estimated elevation of each plant location using the IDW method.

Following the methods described in section 2.6, we determined that the distribution of environmental conditions was similar across the five seeding rates. The mean value of the first quartile of EC_a in each seeding rate is 6.63 with a standard deviation of 0.48, and the third quartile is 10.02 with a standard deviation of 0.44. The mean value of the first quartile of elevation in each seeding rate is 87.52 m with a standard deviation of 0.01, and the third quartile is 87.86 with a standard deviation of 0.01. The ANOVA test shows a statistically significant difference ($p \leq 0.01$) in soil EC_a and elevation between the top 10 % and the bottom 10 % stand count of cotton plants in 5-meter segments at each seeding

rate. Moreover, using the “lm” function in R, we found that both soil EC_a and field elevation were statistically related ($p \leq 0.01$) to the stand count at each seeding rate, with both independent variables having a positive coefficient on the number of plants in 5-meter segments. In addition, the random forest (RF) algorithm found a non-linear relationship between seeding rates and environmental factors. According to Table 5, the average R^2 for the nonlinear regression model across the five seeding rates was 0.62, which is higher than the linear regression model.

3.4. Assessing plant spacing uniformity under varied treatments

Comparing the target cotton seeding rate (seeds ha⁻¹) and the measured stand count (plants ha⁻¹) shows that the overall plant establishment rates (i.e., stand count/target seeding rate) were consistently between 52.8 % and 59.1 % across all seeding rates (Table 6). The lower-than-expected establishment rates are hypothesized to be a result of drought stress at the time of planting.

By following section 2.6, the data of elevation and soil EC_a were divided into quintiles, with the lower quintile representing the lower numerical value of soil EC_a and field elevation. A lower CV indicates greater uniformity. Fig. 10a illustrates that cotton plants in lower EC_a areas (percentile 0 to 20) tended to exhibit better spacing uniformity than other areas, possibly due to soils with less clay content, allowing for easier seed placement and better conditions for germination and emergence. On the other hand, lower elevation areas exhibited less uniformity (Fig. 10b; percentile 0 to 20), potentially due to accumulated water creating unfavorable conditions for germination.

The order of uniformity when averaging the values of the five percentiles is as follows: 56 k, 74 k, 91 k, 108 k, and 123 k, with seeding rates 123 k and 108 k performing better and similarly. Additionally, it is also important to identify the optimal cotton seeding rate for achieving uniform emergence in fields with varying ground conditions. According to Fig. 10, the 56 k seeding rate performed well under some specific environmental conditions. According to Mississippi Extension (Dodds, 2023), it is generally recommended that the final plant population for cotton be between 98,840 and 111,200 seeds per acre, which equates to 10–11 cotton plants per meter. Another report (Adams et al., 2019) suggests that using a seeding rate 20 percent higher than the desired final plant population should be considered since some seeds may not germinate. These two recommendations are consistent with our findings that 108 k and 123 k seeding rate ha⁻¹ provide optimal output under average of various environmental conditions.

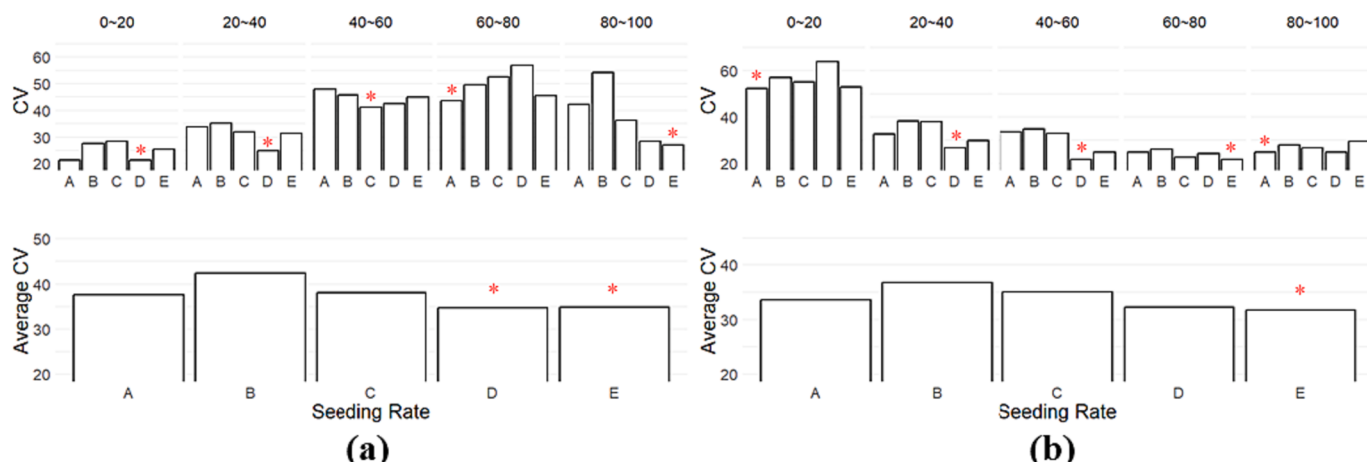


Fig. 10. The coefficient of variation in seeding rate across environmental factors is evenly divided into five percentile ranges. (a) Soil EC_a. (b) field elevation. The asterisk (*) indicates the lowest CV value, meaning the greatest uniformity. Letters A, B, C, D, and E represent seeding rates of 56 k, 74 k, 91 k, 108 k, and 123 k.

4. Conclusion and Future research

This study applied a UAV as a remote sensing platform combined with deep learning and statistical analysis to evaluate cotton uniformity under five seeding rates, two cultivars, and a range of soil properties found within a field. Our results provide an evaluation of five levels of seeding rates based on different elevations and soil conditions across the field, providing a high-throughput approach. By applying the coefficient of variance as the criteria, we concluded that the seeding rates of 108 k and 123 k seeds ha^{-1} had better emergence spacing uniformity than seeding rates of 56 k, 74 k, and 91 k. Future studies could focus on combining emergence data from multiple years, taking into account not only soil characteristics and elevation, but also the weather before and after the planting date each year. It is also worth investigating the statistical relationship between yield and seedling uniformity over multiple years of data. This information could be used to create a planting prescription map for variable rate planters, ultimately increasing yield. In addition, to achieve a higher accuracy of cotton stand count, more object detection models should be evaluated. Based on precision agriculture techniques, this study has provided valuable insights that could help farmers and researchers manage their fields more efficiently and ultimately improve crop production.

CRediT authorship contribution statement

Fengkai Tian: Writing – review & editing, Writing – original draft, Methodology, Investigation, Formal analysis, Data curation. **Curtis J. Ransom:** Writing – review & editing, Resources, Conceptualization. **Jianfeng Zhou:** Writing – review & editing, Supervision, Project administration, Methodology, Funding acquisition, Formal analysis, Conceptualization. **Bradley Wilson:** Resources, Data curation, Conceptualization. **Kenneth A. Sudduth:** Writing – review & editing, Resources, Funding acquisition, Conceptualization.

Declaration of Competing Interest

The authors declare that they have no known competing financial interests or personal relationships that could have appeared to influence the work reported in this paper.

Data availability

Data will be made available on request.

Acknowledgments

The authors would like to thank the University of Missouri—Fisher Delta Research, Extension, and Education Center. The authors would also like to extend their gratitude to the funding agencies that supported this research provided by USDA-ARS NACA.

References

- Adams, C., Thapa, S., Kimura, E., 2019. Determination of a plant population density threshold for optimizing cotton lint yield: a synthesis. *Field Crop Res.* 230, 11–16.
- L.S. Agisoft Agisoft photoscan pro 2014 Petersburg, Russia Disponível em: <http://www.agisoft.com>.
- Bouguettaya, A., Zarzour, H., Kechida, A., Taberkit, A.M., 2022. Deep learning techniques to classify agricultural crops through UAV imagery: a review. *Neural Comput. & Appl.* 34 (12), 951–956.
- Brown, C.E., 1998. Coefficient of variation. In *Applied multivariate statistics in geohydrology and related sciences*. Springer, pp. 155–157.
- S.R. Butler Tyson Making the cotton replant decision 2019.
- Diwan, T., Anirudh, G., Tembhurane, J.V., 2023. Object detection using YOLO: challenges, architectural successors, datasets and applications. *Multimed. Tools Appl.* 82 (6), 9243–9275.
- D. Dodds What is the recommended seeding rate for cotton? Retrieved 04/12 from <http://extension.msstate.edu/content/what-the-recommended-seeding-rate-for-cotton>.
- Duda, R.O., Hart, P.E., 1972. Use of the Hough transformation to detect lines and curves in pictures. *Commun. ACM.* 15 (1), 11–15.
- Dwyer, B., & Nelson, J. (2022). Roboflow (version 1.0). URL <https://roboflow.com>.
- Feng, A., Zhou, J., Vories, E., Sudduth, K.A., 2020. Evaluation of cotton emergence using UAV-based imagery and deep learning. *Comput. Electron. Agric.* 177, 105711.
- Feng, A., Zhou, J., Vories, E., Sudduth, K.A., 2023. Prediction of cotton yield based on soil texture, weather conditions and UAV imagery using deep learning. *Precis. Agric.* 1–24.
- Friedman, S.P., 2005. Soil properties influencing apparent electrical conductivity: a review. *Comput. Electron. Agric.* 46 (1–3), 45–70.
- Fuentes-Peñaillilo S. Ortega-Farías D. de la Fuente-Sáiz M. Rivera (2019). Digital count of sunflower plants at emergence from very low altitude using UAV images. IEEE CHILEAN Conference on Electrical 2019 Electronics Engineering Information and Communication Technologies (CHILECON).
- Gallo, I., Rehman, A.U., Dehkordi, R.H., Landro, N., La Grassa, R., Boschetti, M., 2023. Deep object detection of crop weeds: performance of YOLOv7 on a real case dataset from UAV images. *Remote Sens. (Basel.)* 15 (2), 539. <https://www.mdpi.com/2072-4929/15/2/539>.
- Harper, J., Williams, J., Sagar, G., 1965. The heterogeneity of soil surfaces and its role in determining the establishment of plants from seed. *J. Ecol.* 53, 273–286.
- Jin, X., Liu, S., Baret, F., Hemerlé, M., Comar, A., 2017. Estimates of plant density of wheat crops at emergence from very low altitude UAV imagery. *Remote Sens. Environ.* 198, 105–114.
- Kaivosaaja, J., Hautsalo, J., Heikkilä, J., Hiltunen, L., Ruuttunen, P., Näsi, R., Niemeläinen, O., Lemslau, M., Honkavaara, E., Salonen, J., 2021. Reference measurements in developing UAV Systems for detecting pests, weeds, and diseases. *Remote Sens. (Basel.)* 13 (7), 1238.
- Khan, S., Tufail, M., Khan, M.T., Khan, Z.A., Iqbal, J., Alam, M., 2021. A novel semi-supervised framework for UAV based crop/weed classification. *PLoS One.* 16 (5), e0251008.
- Kholliyev, A.E., Norboyeva, U.T., Kholov, Y.D., Boltayeva, Z.A., 2020. Productivity of cotton varieties in soil salinity and water deficiency. *American J. Applied Sci.* 2 (10), 7–13.
- Li, B., Xu, X., Han, J., Zhang, L., Bian, C., Jin, L., Liu, J., 2019. The estimation of crop emergence in potatoes by UAV RGB imagery. *Plant Methods.* 15 (1), 1–13.
- Liliane, T.N., Charles, M.S., 2020. Factors affecting yield of crops. In: *Agronomy–Climate Change & Food Security*, p. 9.
- Liu, S., Baret, F., Allard, D., Jin, X., Andrieu, B., Burger, P., Hemerlé, M., Comar, A., 2017. A method to estimate plant density and plant spacing heterogeneity: application to wheat crops. *Plant Methods.* 13 (1), 1–11.
- Liu, W., Zhou, J., Wang, B., Costa, M., Kaepller, S.M., Zhang, Z., 2022. IntegrateNet: a deep learning network for maize stand counting from UAV imagery by integrating density and local count maps. *IEEE Geosci. Remote Sens. Lett.* 19, 1–5.
- P. Lottes R. Khanna J. Pfeifer R. Siegwart C. Stachniss UAV-based crop and weed classification for smart farming 2017 IEEE International Conference on Robotics and Automation (ICRA) 2017.
- Maes, W.H., Steppé, K., 2019. Perspectives for remote sensing with unmanned aerial vehicles in precision agriculture. *Trends Plant Sci.* 24 (2), 152–164.
- Oosterhuis, D.M., 1990. Growth and development of a cotton plant. Practical issues, Nitrogen nutrition of cotton, pp. 1–24.
- Padilla, R., Passos, W.L., Dias, T.L., Netto, S.L., Da Silva, E.A., 2021. A comparative analysis of object detection metrics with a companion open-source toolkit. *Electronics.* 10 (3), 279.
- S. Panigrahy S. Karmakar Research on Transmission Line Insulator Defects Detection using YOLOv7 2022 IEEE 6th International Conference on Condition Assessment Techniques in Electrical Systems (CATCON) 2022.
- Pedregosa, F., Varoquaux, G., Gramfort, A., Michel, V., Thirion, B., Grisel, O., Blondel, M., Prettenhofer, P., Weiss, R., Dubourg, V., 2011. Scikit-learn: machine learning in Python. *J. Machine Learning Res.* 12, 2825–2830.
- Qiao, P., Lei, M., Yang, S., Yang, J., Guo, G., Zhou, X., 2018. Comparing ordinary kriging and inverse distance weighting for soil as pollution in Beijing. *Environ. Sci. Pollut. Res.* 25, 15597–15608.
- H. Rezatofighi N. Tsai J. Gwak A. Sadeghian I. Reid S. Savarese Generalized intersection over union: A metric and a loss for bounding box regression Proceedings of the IEEE/CVF Conference on Computer Vision and Pattern Recognition 2019.
- Sankaranarayanan, K., Praharaj, C., Nalayini, P., Bandyopadhyay, K., & Gopalakrishnan, N. (2010). Climate change and its impact on cotton.
- Sharma, A., Jain, A., Gupta, P., Chowdary, V., 2020. Machine learning applications for precision agriculture: a comprehensive review. *IEEE Access.* 9, 4843–4873.
- Sonon, L. S., Saha, U., & Kissel, D. E. (2015). Soil salinity. *Testing, data interpretation and recommendations. Circular,* 1019.
- Sudduth, K.A., Kitchen, N., Boller, G., Bullock, D., Wiebold, W., 2003. Comparison of electromagnetic induction and direct sensing of soil electrical conductivity. *Agron. J.* 95 (3), 472–482.
- Tetila, E.C., Machado, B.B., Astolfi, G., de Souza Belete, N.A., Amorim, W.P., Roel, A.R., Pistori, H., 2020. Detection and classification of soybean pests using deep learning with UAV images. *Comput. Electron. Agric.* 179, 105836.
- Tian, F., Vieira, C.C., Zhou, J., Chen, P., 2023. Estimation of off-target dicamba damage on soybean using UAV imagery and deep learning. *Sensors.* 23 (6), 3241.
- Tsouros, D.C., Bibi, S., Sarigiannidis, P.G., 2019. A review on UAV-based applications for precision agriculture. *Information.* 10 (11), 349. <https://www.mdpi.com/2078-2489/10/11/349>.
- Vong, C.N., Conway, L.S., Zhou, J., Kitchen, N.R., Sudduth, K.A., 2021. Early corn stand count of different cropping systems using UAV-imagery and deep learning. *Comput. Electron. Agric.* 186, 106214.

- Walker, M., 2023. 2023. Consumption Rebounds but Economic Pressure Remains, World Cotton Outlook <https://www.cotton.org/news/meetings/2023annual/ecjo.cfm>.
- Wang, C.-Y., Bochkovskiy, A., & Liao, H.-Y. M. (2022). YOLOv7: Trainable bag-of-freebies sets new state-of-the-art for real-time object detectors. *arXiv preprint arXiv:2207.02696*.
- Wang, L., Xiang, L., Tang, L., Jiang, H., 2021. A convolutional neural network-based method for corn stand counting in the field. *Sensors.* 21 (2), 507.
- Zhang, L., Zhang, H., Niu, Y., Han, W., 2019. Mapping maize water stress based on UAV multispectral remote sensing. *Remote Sens. (Basel).* 11 (6), 605.
- Zhang, J., Zhao, B., Yang, C., Shi, Y., Liao, Q., Zhou, G., Wang, C., Xie, T., Jiang, Z., Zhang, D., 2020a. Rapeseed stand count estimation at leaf development stages with UAV imagery and convolutional neural networks. *Front. Plant Sci.* 11, 617. <https://www.sciencedirect.com/science/article/pii/S153751101930875X>.
- Zhang, M., Zhou, J., Sudduth, K.A., Kitchen, N.R., 2020b. Estimation of maize yield and effects of variable-rate nitrogen application using UAV-based RGB imagery. *Biosyst. Eng.* 189, 24–35. <https://doi.org/10.3389/fpls.2020.00617>.